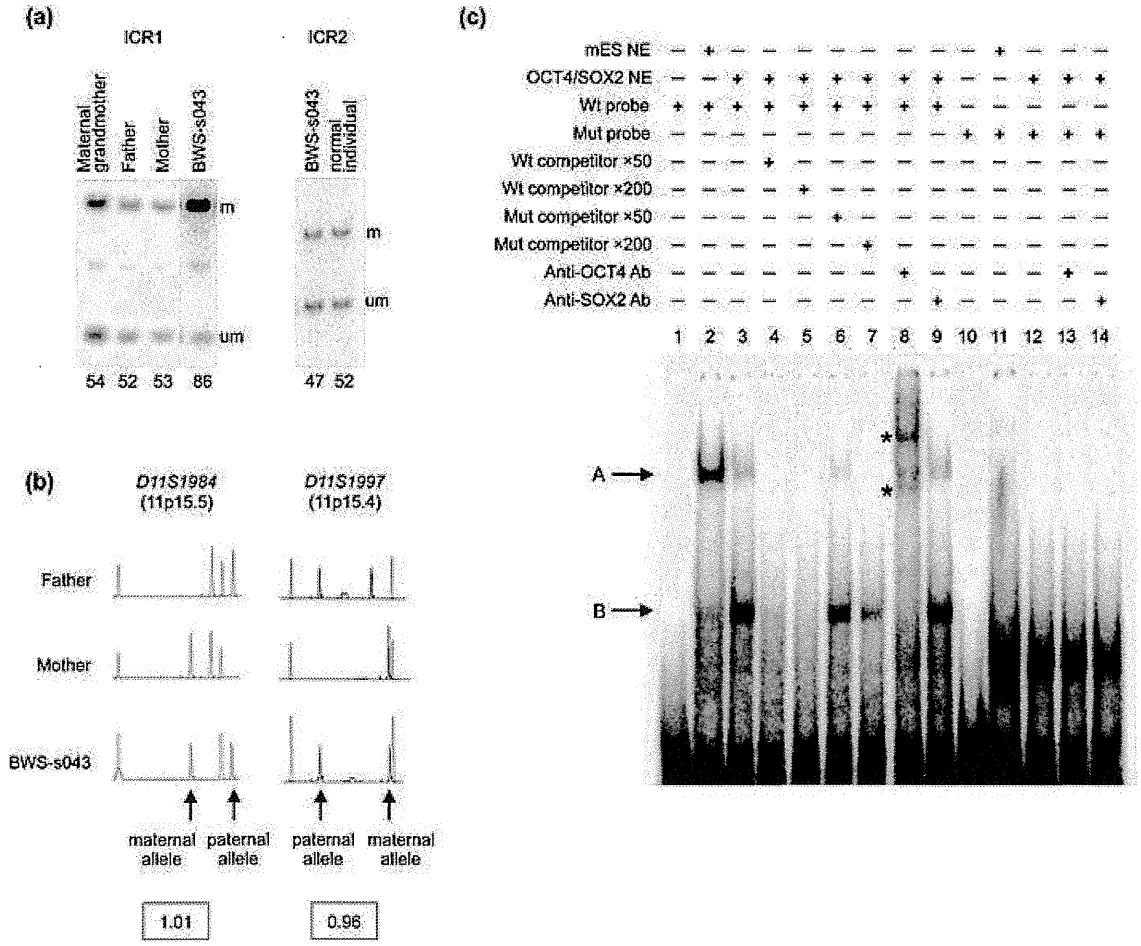

Fig. 2. Methylation-sensitive Southern blots and microsatellite analysis of BWS-s043, and electrophoretic mobility shift assay (EMSA) for 2,023,018C>T. (**a**) Methylation-sensitive Sothern blots of ICR1 and ICR2. Methylation indices [MI, %] are shown below each lane. MI was calculated using the equation $M/(M+U) \times 100$, where M is the intensity of the methylated band and U is the intensity of the unmethylated band. m, methylated band; um, unmethylated band. BWS-s043 showed ICR1-GOM, whereas the relatives did not. Methylation statuses of CTS1 and CTS4 are shown in Fig. S2b,c. Methylation of ICR2 in BWS-s043 was normal. (**b**) Microsatellite analysis at 11p15.4-p15.5. Ratios of the paternal allele to the maternal allele in BWS-s043 were approximately 1, indicating no uniparental disomy. Red peaks are molecular markers. (**c**) EMSA using the wild-type (Wt) probe and the mutant (Mut) probe encompassing 2,023,018C>T. The unlabeled Wt probe or Mut probe (×50 or ×200 molar excess) was used as a competitor. The arrows and asterisks indicate the protein-DNA complexes (A and B) and supershifted complexes, respectively. mES NE, nuclear extract from mouse ES cells; OCT4/SOX2 NE, nuclear extract from human HEK293 cells expressing OCT4/SOX2; Ab, antibody.

for BWS-s043, were not located at any protein-binding sites that have been reported as involved in methylation imprinting (CTCF, OCT, and ZFP57) (3, 4, 10, 12, 16). Furthermore, we did not find any protein-oligonucleotide complexes in EMSA using mouse ES nuclear extracts and oligonucleotide probes encompassing all variants, except for BWS-s043 (Fig. S1). Therefore, we analyzed further three variants in BWS-s043, which were in and around the OCT-binding site 1.

First, we re-confirmed that BWS-s043 showed GOM near CTS6 within ICR1, but it did not demonstrate LOM at ICR2, paternal uniparental disomy of chromosome 11, or a *CDKN1C* mutation (Fig. 2a,b, and data not shown). The 2,023,018C>T variant was located in the second octamer motif of OCT-binding site 1 within repeat A2 (Fig. 1a). The other two variants were located approximately 450 bp on the telomeric side of the 2,023,018C>T variant, between repeats A2 and B4 (Fig. 1a, Table 1). The 2,023,018C>T variant was absent in other family members, indicating a *de novo* variant (Fig. 1a). To clarify if the *de novo* variant in the patient occurred on the maternal or paternal allele, we performed haplotype analysis with PCR covering all three variants. We found all three variants were located on the same allele and the 2,023,018C>T variant occurred *de novo* on the maternal allele because the 2,022,561–562CT>delCT and 2,022,565G>C variants were on the maternal allele in the patient (Fig. 1b,c).

Next, we investigated the methylation status of ICR1. Methylation-sensitive Southern blots and bisulfite sequencing showed normal methylation of ICR1 in the parents and the maternal grandmother (Figs 2a and S2). As for the 2,022,561-562CT>delCT and the 2,022,565G>C variants, the variant allele was unmethylated in the mother, but methylated in the grandmother (Fig. 1d). On the basis of methylation

analysis, the variant allele in the grandmother must have been transmitted by her father, and that in the mother must have been transmitted by her mother. The results indicated that the variant allele could be either methylated or unmethylated during gametogenesis, strongly suggesting no relation between the variants and ICR1-GOM. On the other hand, bisulfite sequencing including the 2,023,018C>T variant revealed that both the variant and wild-type alleles were heavily methylated in the patient (Fig. 1e), while differential methylation was maintained in other family members and normal controls without the variant (Fig. S2a). As the *de novo* variant on the maternal allele was located within the OCT-binding site, which is required for the maintenance of the unmethylated status in a mouse model, the variant was likely involved in ICR1-GOM (17, 18).

Finally, we performed EMSA to determine if 2,023,018C>T influenced the binding ability of nuclear protein factors, such as OCT4 and SOX2 (Fig. 2c). The wild-type probe formed two complexes (A and B) with the nuclear extracts of mouse ES cells and HEK293 cells expressing OCT4/SOX2 (lanes 2 and 3), whereas such complexes were not observed in the mutant probe (lanes 11 and 12). Complexes A and B competed more efficiently with wild-type than with the mutant competitor (lanes 4 to 7). Furthermore, complex B, but not A, was supershifted with the antibody against OCT4 (lane 8). The supershift did not occur with the antibody against SOX2 and with both antibodies using the mutant probe (lanes 9, 13, and 14). These data demonstrated that 2,023,018C>T abrogated binding ability of a nuclear factor, most likely OCT4. Taken together, our data strongly suggest that 2,023,018C>T is a mutation that could prevent OCT4 binding to the OCT-binding site and induce ICR1-GOM, leading to BWS.

Discussion

We identified a novel *de novo* point mutation, chr11: 2,023,018C>T, in OCT-binding site 1 within repeat A2 in a BWS patient with ICR1-GOM. Our data strongly suggest the involvement of the mutation in GOM at ICR1. In a mouse cell model, the evolutionarily well-conserved dyad octamer motif within ICR1, which is bound by OCT protein, has been shown to be required for the maintenance of unmethylated status competing against *de novo* methylation (17). In addition, the importance of a SOX motif flanked by an OCT motif has also been reported (19). Recent studies have shown that the SOX–OCT motif functions to maintain unmethylated status *in vitro* and *in vivo*; a cooperative function of CTCF and OCT/SOX for maintenance of differential methylation has been suggested as responsible (18, 19). Although there is one OCT-binding site in mice, three evolutionarily conserved OCT-binding sites (0, 1, 2) are located in and around ICR1 in humans. As all mutations and the small deletion previously reported in addition to our case occurred in site 1 within repeat A2 (Fig. 1a), site 1 within repeat A2 likely plays a more important role for maintaining unmethylated status of maternal ICR1 in humans than the other OCT-binding sites (10, 12, 13).

ICR1-GOM cases, including ours, with mutations/deletions also show partial hypermethylation in spite of pre-existent genetic aberrations in the oocyte (9, 12, 13, 20), suggesting aberrant hypermethylation at ICR1 would also be stochastically acquired at a cellular level even in the existence of such aberrations.

As for SRS, including familial cases, the ICR1 mutation has not been found except in one sporadic case to date (10). We did not find any promising mutations in this study, suggesting the cause of ICR1 methylation defects to differ between SRS and BWS.

In conclusion, we identified a novel *de novo* point mutation of OCT-binding site 1 within repeat A2, a location suggested to play an important role for maintaining the unmethylated status of maternal ICR1 in humans, on the maternal allele in a BWS patient with ICR1-GOM. However, genetic aberrations of ICR1 explain only 20% of BWS cases with ICR1-GOM (10). As aberrant methylation may occur as a consequence of stochastic events or environmental influences irrespective of ICR1 mutations, unknown causes for ICR1 methylation defects should be clarified.

Supporting Information

The following Supporting information is available for this article:

Fig. S1. EMSA for all variants found in this study, except for those in BWS-047 and BWS-s061, using the nuclear extract from mouse ES cells. The variant in BWS-s081 was located outside of ICR1, and a CpG site within the probe sequence was mostly unmethylated in three normal controls (data not shown). Thus, an unmethylated probe was used for it. Since the variants in BWS-s100 and SRS-s03 were located 3′ of CTS6 and found on the maternal allele, unmethylated probes were used for them. As for the variant in SRS-002, it was located 5′ of CTS1 but its parental origin was unknown. Thus, both unmethylated and methylated probes were used for it. There was no difference between a wt-probe and a variant-probe in each variant except for the BWS-s043 mutation. A wt-probe for the BWS-s043 mutation formed two complexes, whereas such complexes were not observed with a probe for the mutation. These results suggested that only the BWS-s043 mutation affected the protein–DNA interaction (see text and Fig. 2c for details). WT, probe for the wild-type sequence; MUT, probe for the BWS-s043 mutation; VAR, probe for the variant sequence; um, unmethylated probe; me, methylated probe; mES NE, nuclear extract from mouse ES cells.
Fig. S2. Bisulfite sequencing of the region encompassing the 2,023,018 variant, CTS1, and CTS4. (**a**) Results for the 2,023,018 variant. In the healthy members of the BWS-s043 family, comprised of the maternal grandmother, mother, and father, showed differential methylation. Three normal controls also showed differential methylation. In particular, normal control 3 was heterozygous for a SNP (rs61520309) and showed differential methylation in an allele-dependent manner. Open and filled circles indicate unmethylated and methylated CpG sites, respectively. (**b**) Results for CTS1. Two normal controls that were heterozygous for a SNP (rs2525885) showed differential methylation. The healthy family members also showed differential methylation, whereas the patient, BWS-s043, showed aberrant hypermethylation. CpG sites within CTS1 are indicated by a short horizontal line. X indicates T of the SNP (rs2525885). (**c**) Results for CTS4. The healthy family members and two normal controls showed differential

methylation. Among them, the parents and two normal controls were heterozygous for a SNP (rs2525883). The patient, BWS-s043, showed aberrant hypermethylation. CpG sites within CTS4 were indicated by a short horizontal line. X indicates T of the SNP (rs2525883).
Table S1. PCR primers and oligonucleotide probes used in this study.

Additional Supporting information may be found in the online version of this article.

Acknowledgements

This study was supported, in part, by a Grant for Research on Intractable Diseases from the Ministry of Health, Labor, and Welfare; a Grant for Child Health and Development from the National Center for Child Health and Development; a Grant-in-Aid for Challenging Exploratory Research; and, a Grant-in-Aid for Scientific Research (C) from the Japan Society for the Promotion of Science.

References

1. Weksberg R, Shuman C, Beckwith JB. Beckwith–Wiedemann syndrome. Eur J Hum Genet 2010: 18: 8–14.
2. Gicquel C, Rossignol S, Cabrol S et al. Epimutation of the telomeric imprinting center region on chromosome 11p15 in Silver–Russell syndrome. Nat Genet 2005: 37: 1003–1007.
3. Bell AC, Felsenfeld G. Methylation of a CTCF-dependent boundary controls imprinted expression of the Igf2 gene. Nature 2000: 405: 482–485.
4. Hark AT, Schoenherr CJ, Katz DJ, Ingram RS, Levorse JM, Tilghman SM. CTCF mediates methylation-sensitive enhancer-blocking activity at the H19/Igf2 locus. Nature 2000: 405: 486–489.
5. Schoenherr CJ, Levorse JM, Tilghman SM. CTCF maintains differential methylation at the Igf2/H19 locus. Nat Genet 2003: 33: 66–69.
6. Pant V, Mariano P, Kanduri C et al. The nucleotides responsible for the direct physical contact between the chromatin insulator protein CTCF and the H19 imprinting control region manifest parent of origin-specific long-distance insulation and methylation-free domains. Genes Dev 2003: 17: 586–590.
7. Sparago A, Cerrato F, Vernucci M, Ferrero GB, Silengo MC, Riccio A. Microdeletions in the human H19 DMR result in loss of IGF2 imprinting and Beckwith–Wiedemann syndrome. Nat Genet 2004: 36: 958–960.
8. Prawitt D, Enklaar T, Gärtner-Rupprecht B et al. Microdeletion of target sites for insulator protein CTCF in a chromosome 11p15 imprinting center in Beckwith–Wiedemann syndrome and Wilms' tumor. Proc Natl Acad Sci U S A 2005: 102: 4085–4090.
9. Beygo J, Citro V, Sparago A et al. The molecular function and clinical phenotype of partial deletions of the IGF2/H19 imprinting control region depends on the spatial arrangement of the remaining CTCF-binding sites. Hum Mol Genet 2013: 22: 544–557.
10. Demars J, Shmela ME, Rossignol S et al. Analysis of the IGF2/H19 imprinting control region uncovers new genetic defects, including mutations of OCT-binding sequences, in patients with 11p15 fetal growth disorders. Hum Mol Genet 2010: 19: 803–814.
11. Quenneville S, Verde G, Corsinotti A et al. In embryonic stem cells, ZFP57/KAP1 recognize a methylated hexanucleotide to affect chromatin and DNA methylation of imprinting control regions. Mol Cell 2011: 44: 361–372.
12. Poole RL, Docherty LE, Al Sayegh A et al. Targeted methylation testing of a patient cohort broadens the epigenetic and clinical description of imprinting disorders. Am J Med Genet A 2013: 161: 2174–2182.
13. Berland S, Appelbäck M, Bruland O et al. Evidence for anticipation in Beckwith–Wiedemann syndrome. Eur J Hum Genet 2013: 21: 1344–1348.
14. Higashimoto K, Nakabayashi K, Yatsuki H et al. Aberrant methylation of H19-DMR acquired after implantation was dissimilar in soma versus placenta of patients with Beckwith–Wiedemann syndrome. Am J Med Genet A 2012: 158A: 1670–1675.
15. Soejima H, Nakagawachi T, Zhao W et al. Silencing of imprinted CDKN1C gene expression is associated with loss of CpG and histone H3 lysine 9 methylation at DMR-LIT1 in esophageal cancer. Oncogene 2004: 23: 4380–4388.
16. Mackay DJ, Callaway JL, Marks SM et al. Hypomethylation of multiple imprinted loci in individuals with transient neonatal diabetes is associated with mutations in ZFP57. Nat Genet 2008: 40: 949–951.
17. Hori N, Nakano H, Takeuchi T et al. A dyad Oct-binding sequence functions as a maintenance sequence for the unmethylated state within the H19/Igf2-imprinted control region. J Biol Chem 2002: 277: 27960–27967.
18. Sakaguchi R, Okamura E, Matsuzaki H, Fukamizu A, Tanimoto K. Sox-Oct motifs contribute to maintenance of the unmethylated H19 ICR in YAC transgenic mice. Hum Mol Genet 2013: 22: 4627–4637.
19. Hori N, Yamane M, Kouno K, Sato K. Induction of DNA demethylation depending on two sets of Sox2 and adjacent Oct3/4 binding sites (Sox-Oct motifs) within the mouse H19/insulin-like growth factor 2 (Igf2) imprinted control region. J Biol Chem 2012: 287: 44006–44016.
20. Sparago A, Russo S, Cerrato F et al. Mechanisms causing imprinting defects in familial Beckwith–Wiedemann syndrome with Wilms' tumour. Hum Mol Genet 2007: 16: 254–264.

Clinical Endocrinology (2013) doi: 10.1111/cen.12379

ORIGINAL ARTICLE

IMAGe syndrome: clinical and genetic implications based on investigations in three Japanese patients

Fumiko Kato*, Takashi Hamajima†, Tomonobu Hasegawa‡, Naoko Amano‡, Reiko Horikawa§, Gen Nishimura¶, Shinichi Nakashima*, Tomoko Fuke**, Shinichirou Sano**, Maki Fukami** and Tsutomu Ogata*

*Department of Pediatrics, Hamamatsu University School of Medicine, Hamamatsu, †Division of Endocrinology and Metabolism, Aichi Children's Health and Medical Center, Obu, ‡Department of Pediatrics, Keio University School of Medicine, §Division of Endocrinology and Metabolism, National Center for Child Health and Development, Tokyo, ¶Department of Radiology, Tokyo Metropolitan Children's Medical Center, Fuchu, and **Department of Molecular Endocrinology, National Research Institute for Child Health and Development, Tokyo, Japan

Summary

Objective Arboleda *et al.* have recently shown that IMAGe (intra-uterine growth restriction, metaphyseal dysplasia, adrenal hypoplasia congenita and genital abnormalities) syndrome is caused by gain-of-function mutations of maternally expressed gene *CDKN1C* on chromosome 11p15.5. However, there is no other report describing clinical findings in patients with molecularly studied IMAGe syndrome. Here, we report clinical and molecular findings in Japanese patients.

Patients We studied a 46,XX patient aged 8·5 years (case 1) and two 46,XY patients aged 16·5 and 15·0 years (cases 2 and 3).

Results Clinical studies revealed not only IMAGe syndrome-compatible phenotypes in cases 1–3, but also hitherto undescribed findings including relative macrocephaly and apparently normal pituitary-gonadal endocrine function in cases 1–3, familial glucocorticoid deficiency (FGD)-like adrenal phenotype and the history of oligohydramnios in case 2, and arachnodactyly in case 3. Sequence analysis of *CDKN1C*, pyrosequencing-based methylation analysis of KvDMR1 and high-density oligonucleotide array comparative genome hybridization analysis for chromosome 11p15.5 were performed, showing an identical *de novo* and maternally inherited *CDKN1C* gain-of-function mutation (p.Asp274Asn) in cases 1 and 2, respectively, and no demonstrable abnormality in case 3.

Conclusions The results of cases 1 and 2 with *CDKN1C* mutation would argue the following: [1] relative macrocephaly is consistent with maternal expression of *CDKN1C* in most tissues and biparental expression of *CDKN1C* in the foetal brain; [2] FGD-like phenotype can result from *CDKN1C* mutation; and [3] genital abnormalities may primarily be ascribed to placental dysfunction. Furthermore, lack of *CDKN1C* mutation in case 3 implies genetic heterogeneity in IMAGe syndrome.

(Received 1 October 2013; returned for revision 24 November 2013; finally revised 26 November 2013; accepted 29 November 2013)

Correspondence: Dr. Tsutomu Ogata, Department of Pediatrics, Hamamatsu University School of Medicine, 1-20-1 Handayama, Higashi-ku, Hamamatsu 431-3192, Japan. Tel./Fax: +81 53 435 2310;
E-mail: tomogata@hama-med.ac.jp

Introduction

IMAGe syndrome is a multisystem developmental disorder named by the acronym of intra-uterine growth restriction (IUGR), metaphyseal dysplasia and adrenal hypoplasia congenita common to both 46,XY and 46,XX patients, and genital abnormalities specific to 46,XY patients.[1] In addition to these salient clinical features, hypercalciuria has been reported frequently in IMAGe syndrome.[1,2] This condition occurs not only as a sporadic form but also as a familial form.[1–3] Furthermore, transmission analysis in a large pedigree has revealed an absolute maternal inheritance of this condition, indicating the relevance of a maternally expressed gene to the development of IMAGe syndrome.[3]

Subsequently, Arboleda *et al.*[4] have mapped the causative gene to a ~17·2-Mb region on chromosome 11 by an identity-by-descent analysis in this large pedigree and performed targeted exon array capture and high-throughput genomic sequencing for this region in the affected family members and in other sporadic patients. Consequently, they have identified five different missense mutations in the maternally expressed gene *CDKN1C* (cyclin-dependent kinase inhibitor 1C) that resides on the imprinting control region 2 (ICR2) domain at chromosome 11p15.5 and encodes a negative regulator for cell proliferation.[4–6] Notably, all the missense mutations are clustered within a specific segment of PCNA-binding domain, and functional studies have implicated that these mutations have gain-of-function effects.[4] Thus, IMAGe syndrome appears to constitute a mirror image of Beckwith–Wiedemann syndrome (BWS) in terms of the

CDKN1C function, because multiple *CDKN1C* loss-of-function mutations have been identified in BWS with no mutation shared in common by IMAGe syndrome and BWS.[4,5]

However, several matters remain to be clarified in IMAGe syndrome, including phenotypic spectrum and underlying mechanism(s) for the development of each phenotype in *CDKN1C*-mutation-positive patients, and the presence or absence of genetic heterogeneity. Here, we report clinical and molecular findings in three patients with IMAGe syndrome and discuss these unresolved matters.

Patients and methods

Patients

We studied one previously described 46,XX patient (case 1)[7] and two hitherto unreported 46,XY patients (cases 2 and 3). In cases 1–3, no pathologic mutations were identified in the coding exons and their splice cites of *NR5A1* (*SF1*) and *NR0B1* (*DAX1*) relevant to adrenal hypoplasia,[8] and *MC2R, MRAP, STAR* and *NNT* involved in familial glucocorticoid deficiency (FGD).[9]

Ethical approval and samples

This study was approved by the Institutional Review Board Committee at Hamamatsu University School of Medicine. Molecular studies were performed using leucocyte genomic DNA samples of cases 1–3 and the parents of cases 1 and 2, after obtaining written informed consent.

Sequence analysis of CDKN1C

The coding exons 1 and 2 and their flanking splice sites were amplified by polymerase chain reaction (PCR) (Fig. 1a), using primers shown in Table S1. Subsequently, the PCR products were subjected to direct sequencing from both directions on ABI 3130 autosequencer (Life Technologies, Carlsbad, CA, USA). In this regard, if a nucleotide variation were present within the primer-binding site(s), this may cause a false-negative finding because of amplification failure of a mutation-positive allele. Thus, PNCA-binding domain was examined with different primer sets. To confirm a heterozygous mutation, the corresponding PCR products were subcloned with TOPO TA Cloning Kit (Life Technologies), and normal and mutant alleles were sequenced separately.

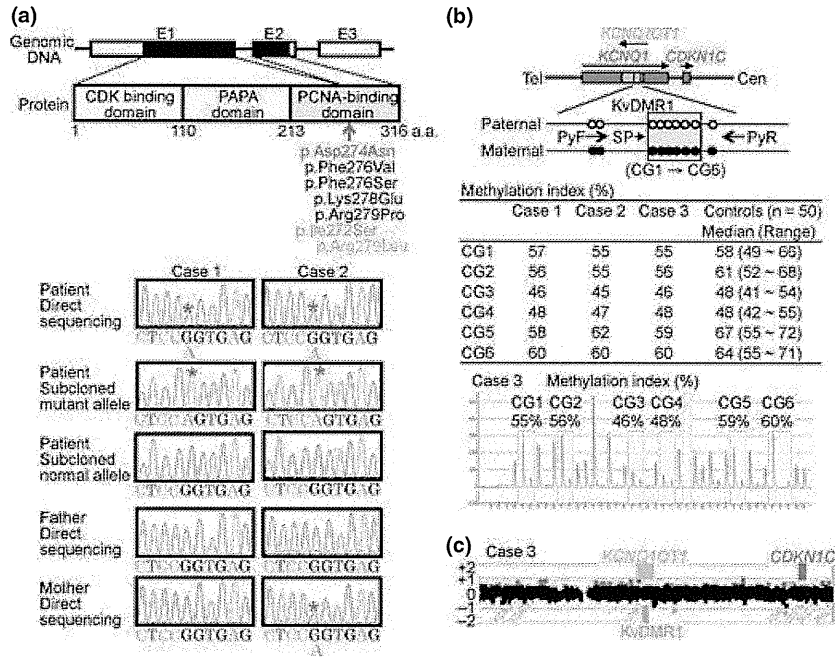

Fig. 1 Summary of molecular studies. (a) Sequence analysis of *CDKN1C*. *CDKN1C* consists of three exons (E1–E3), and the black and white boxes denote the coding regions and the untranslated regions, respectively. CDKN1C protein is composed of 316 amino acids and contains CDK binding domain, PAPA domain and PCNA-binding domain. The p.Asp274Asn mutation found in this study and the previous study[4] is shown in red. The four mutations written in black have also been identified in IMAGe syndrome.[4] The pIle272Ser mutation written in green has been detected in atypical IMAGe syndrome lacking skeletal lesion,[22] and the pArg279Leu mutation written in blue has been found in SRS.[24] Electrochromatograms denote a *de novo* p.Asp274Asn mutation in case 1 and a maternally inherited p.Asp274Asn mutation in case 2. (b) Methylation analysis of KvDMR1 at the ICR2 domain. The cytosine residues at the CpG dinucleotides are unmethylated after paternal transmission (open circles) and methylated after maternal transmission (filled circles). *KCNQ1OT1* is a paternally expressed gene, and *KCNQ1* and *CDKN1C* are maternally expressed genes. The six CpG dinucleotides (CG1→CG6) examined by pyrosequencing are highlighted with a yellow rectangle, and the positions of PyF & PyR primers and SP are shown by thick arrows and a thin arrow, respectively. A pyrogram of case 3 is shown. (c) Array CGH analysis for chromosome 11p15.5 encompassing the ICR2 domain in case 3. A region encompassing KvDMR1 and *CDKN1C* is shown. Black, red and green dots denote signals indicative of the normal, the increased (>+0·5) and the decreased (<−1·0) copy numbers, respectively. Although several red and green signals are seen, there is no portion associated with ≥3 consecutive red or green signals.

Methylation analysis of KvDMR1 and array CGH analysis for chromosome 11p15.5

Increased expression of *CDKN1C*, as well as gain-of-function mutations of *CDKN1C*, may lead to IMAGe syndrome. Such increased *CDKN1C* expression would occur in association with hypermethylated KvDMR1 (differentially methylated region 1) at the ICR2 domain, because *CDKN1C* is expressed when the *cis*-situated KvDMR1 is methylated as observed after maternal transmission and is repressed when the *cis*-situated KvDMR1 is unmethylated as observed after paternal transmission.[5] Thus, we performed pyrosequencing analysis for six CpG dinucleotides (CG1–CG6) within KvDMR1, using bisulphite-treated leucocyte genomic DNA samples (Fig. 1b). In brief, a 155-bp region was PCR-amplified with a primer set (PyF and PyR) for both methylated and unmethylated clones, and a sequence primer (SP) was hybridized to single-stranded PCR products (for PyF, PyR and SP sequences, see Table S1). Subsequently, methylation index (MI, the ratio of methylated clones) was obtained for each CpG dinucleotide, using PyroMark Q24 (Qiagen, Hilden, Germany). To define the reference ranges of MIs, 50 control subjects were similarly studied with permission.

Increased *CDKN1C* expression may also result from a copy number gain of the maternally inherited ICR2 domain. Thus, we performed high-density array CGH (comparative genomic hybridization) using a custom-build 33 088 oligonucleotide probes for chromosome 11p15.5 encompassing the ICR2 domain, together with ~10 000 reference probes for other chromosomal regions (Agilent Technologies, Santa Clara, CA, USA). The procedure was carried out as described in the manufacturer's instructions.

Results

Clinical findings

Detailed clinical findings are shown in Table 1. Cases 1–3 exhibited characteristic faces with frontal bossing, flat nasal root, low set ears and mild micrognathia, as well as short limbs. They had IUGR and postnatal growth failure. Notably, while birth and present length/height and weight were severely compromised, birth and present occipitofrontal circumference (OFC) were relatively well preserved. Radiological examinations revealed generalized osteopenia, delayed bone maturation and metaphyseal dysplasia with vertical sclerotic striations of the knee in cases 1–3, slender bones in cases 1 and 2, scoliosis in cases 2 and 3, arachnodactyly in case 3 and broad distal phalanx of the thumbs and great toes in case 2 (Fig. 2). Cases 1 and 3 experienced adrenal crisis in early infancy and received glucocorticoid and mineralocorticoid supplementation therapy since infancy. Case 2 had transient neonatal hyponatremia and several episodes of hypoglycaemia without electrolyte abnormality in childhood and was found to have hypoglycaemia and hyponatremia without hyperkalemia when he had severe viral gastroenteritis at 15·5 years of age. Thus, an adrenocorticotropic hormone stimulation test was performed after recovery from gastroenteritis, revealing poor cortisol response. Thereafter, he was placed on glucocorticoid supplementation therapy. As serum electrolytes were normal, mineralocorticoid supplementation therapy was not initiated. Genital abnormalities included cryptorchidism and small testes in cases 2 and 3, and hypospadias in case 3. However, pituitary-gonadal endocrine function was apparently normal in cases 1–3. Urine calcium secretion was borderline high or increased in cases 1–3, although serum calcium and calcium homeostasis-related factors were normal. In addition, feeding difficulties during infancy were observed in cases 1 and 2, but not in case 3, and oligohydramnios was noticed during the pregnancy of case 2. There was no body asymmetry in cases 1–3. Thus, clinical studies in cases 1–3 revealed not only IMAGe syndrome-compatible phenotypes, but also hitherto undescribed clinical finding (Table 2).

Sequence analysis of CDKN1C

A heterozygous identical missense mutation (c.820G>A, p.Asp274Asn) was identified in cases 1 and 2 (Fig. 1a). This mutation occurred as a *de novo* event in case 1 and was inherited from the phenotypically normal mother in case 2. No demonstrable mutation was identified in case 3.

Methylation analysis of KvDMR1 and array CGH analysis for chromosome 11p15.5

The MIs for CG1–CG6 were invariably within the normal range in cases 1–3 (Fig. 1b), and no discernible copy number alteration was identified in cases 1–3 (Fig. 1c). The results excluded maternal uniparental disomy involving KvDMR1, hypermethylation (epimutation) of the paternally inherited KvDMR1 and submicroscopic duplication involving the maternally derived ICR2 domain, as well as submicroscopic deletion affecting the paternally derived ICR2 domain.

Discussion

CDKN1C mutations in IMAGe syndrome

We identified a heterozygous *CDKN1C* missense mutation (Asp274Asn) in cases 1 and 2. This mutation has previously been detected in a patient with IMAGe syndrome.[4] Furthermore, *de novo* occurrence of the mutation in case 1 argues for the mutation being pathologic, and maternal transmission of the mutation in case 2 is consistent with *CDKN1C* being a maternally expressed gene. Thus, our results provide further evidence for specific missense mutations of *CDKN1C* being responsible for the development of IMAGe syndrome.

Clinical features in CDKN1C*-mutation-positive cases 1 and 2*

Several matters are noteworthy with regard to clinical findings in *CDKN1C*-mutation-positive cases 1 and 2. First, although

Table 1. Clinical findings of cases 1–3

	Case 1*	Case 2	Case 3
Karyotype	46,XX	46,XY	46,XY
Present age (year)	8·5	16·5	15·0
Characteristic face	Yes	Yes	Yes
Pre- and postnatal growth			
Gestational age (week)	35	37	38
Birth length (cm) (SDS)	37·0 (−3·5)	40·0 (−4·0)	41·0 (−4·3)
Birth weight (kg) (SDS)	1·34 (−2·9)	2·03 (−3·5)	1·71 (−3·4)
Birth OFC (cm) (SDS)	30·7 (−0·3)	32·0 (−0·9)	33·0 (−0·1)
Birth BMI (kg/m^2) (percentile)	9·8 (<3)	12·7 (50)	10·1 (<3)
BMI (kg/m^2) at 2 years of age (SDS)	14·2 (−1·8)	13·0 (−3·4)	Unknown
Present height (cm) (SDS)	92·8 (−6·2)	124·7 (−7·8)	135·2 (−5·1)
Present weight (kg) (SDS)	16·0 (−1·9)	25·4 (−3·5)	30·4 (−2·6)
Present OFC (cm) (SDS)	52·0 (−0·2)	53·0 (−2·5)	Unknown
Present BMI (kg/m^2) (SDS)	18·6 (+1·6)	16·3 (−2·6)	16·6 (−1·7)
Skeletal abnormality			
Examined age (year)	5·5	16·5	15·0
Generalized osteopenia	Yes	Yes	Yes
Delayed maturation	Yes	Yes	Yes
Metaphyseal dysplasia	Yes	Yes	Yes
Slender bones	Yes	Yes	No
Scoliosis	No	Yes	Yes
Arachnodactyly	No	No	Yes
Broad thumbs & big toes	No	Yes	No
Adrenal dysfunction			
Examined age (year) before therapy	0·1 (39 days)	15·5	0·5 (6 months)
MRI/CT	Undetectable	Undetectable	Undetectable
ACTH (pg/ml)	9010 [19·9 ± 8·8]	427 [22·9 ± 6·2]	>1000 [22·9 ± 6·2]
Cortisol (μg/dl)	8·4 [8·3 ± 3·4]	6·9 [9·5 ± 2·9]	<1·0 [9·5 ± 2·9]
After ACTH stimulation†	N.E.	9·4 [> 20]	<1·0 [> 20]
Plasma renin activity (ng/ml/h)	N.E.	6·0 [1·0 ± 0·1]	>25 [1·01 ± 0·14]
Active renin concentration (pg/ml)	21 400 [2·5–21·4]	N.E.	N.E.
Aldosterone (ng/dl)	6·9 [9·7 ± 4·5]	5·2 [8·5 ± 1·4]	4·1 [7·4 ± 2·2]
Na (mEq/l)	122 [135–145]	141 (127‡) [135–145]	126 [135–145]
K (mEq/l)	8·0 [3·7–4·8]	4·2 (4·0‡) [3·7–4·8]	6·5 [3·7–4·8]
Cl (mEq/l)	86 [98–108]	103 (98‡) [98–108]	89 [98–108]
Glucocorticoid therapy	Yes (since 2 months)	Yes (since 15·5 years)	Yes (since 6 months)
Mineralocorticoid therapy	Yes (since 2 months)	No	Yes (since 6 months)
Genital abnormality			
Examined age (year)	8·5	16·5	15·0
Hypospadias	–	No	Yes (operated at 2 years)
Cryptorchidism	–	Yes (B) (operated at 2 years)	Yes (operated at 2 years)
Micropenis	–	No	No
Testis size (R & L) (ml)	–	5 & 8 [13–20]	4 & 10 [11–20]
Pubic hair (Tanner stage)	1 [10·0 ± 1·4 years]§	4 [14·9 ± 0·9 years]¶	4 [14·9 ± 0·9 years]¶
LH (mIU/ml)	<0·1 [<0·1–1·3]	3·9 [0·2–7·8]	4·8 [0·2–7·8]
After GnRH-stimulation**	3·5 [1·6–4·8]	N.E.	N.E.
FSH (mIU/ml)	0·7 [<0·1–5·4]	4·2 [0·3–18·4]	17·6 [0·3–18·4]
After GnRH-stimulation**	12·0 [10·7–38·1]	N.E.	N.E.
Testosterone (ng/ml)	–	4·3 [1·7–8·7]	3·7 [1·7–8·7]
Calcium metabolism			
Examined age (year)	8·5	16·5	15·0
Calcium (mg/dl)	9·7 [8·8–10·5]	9·2 [8·9–10·6]	9·8 [8·9–10·6]
Inorganic phosphate (mg/dl)	3·9 [3·7–5·6]	4·6 [3·1–5·0]	3·8 [3·2–5·1]
Alkaline phosphatase (IU/l)	458 [343–917]	623 [225–680]	309 [225–680]
Intact PTH (pg/ml)	23 [10–65]	43 [10–65]	28 [10–65]
PTHrP (pmol/l)	N.E.	<1·1 [<1·1]	N.E.

(continued)

Table 1. (continued)

	Case 1*	Case 2	Case 3
$1,25(OH)_2$ vitamin D (pg/ml)	50 [13–79]	67 [13–79]	50 [13–79]
Urine calcium/creatinine ratio (mg/mg)	0·82 [<0·25]	0·24 [<0·25]	0·44 [<0·25]
%TRP	92 [80–96]	95 [80–96]	94 [80–96]
Others	Feeding difficulties	Feeding difficulties Oligohydramnios	

SDS, standard deviation score; OFC, occipitofrontal circumference; BMI, body mass index; MRI, magnetic resonance imaging; CT, computed tomography; ACTH, adrenocorticotropic hormone; R, right; L, left; LH, luteinizing hormone; FSH, follicle-stimulating hormone; GnRH, gonadotropin-releasing hormone; PTH, parathyroid hormone; PTHrP, PTH-related protein; TRP, tubular reabsorption of phosphate; N.E., not examined; and B, bilateral.
Biochemical values indicate basal blood values, except for those specifically defined.
Birth and present length/height, weight, OFC and BMI have been assessed by sex- and gestational- or age-matched Japanese reference data reported in the literature[26,27] and in the Ministry of Health, Labor, and Welfare Database (http://www.e-stat.go.jp/SG1/estat/GL02020101.do).
The values in brackets represent age- and sex-matched reference values in Japanese children.[28]
The conversion factor to the SI unit: 0·220 for ACTH (pmol/l), 27·6 for cortisol (nmol/l), 0·028 for aldosterone (nmol/l), 3·46 for testosterone (nmol/l), 0·25 for calcium (nmol/l), 0·323 for inorganic phosphate (nmol/l), 0·106 for intact PTH (pmol/l), 2·40 for $1,25(OH)_2$ vitamin D (pmol/l) and 1·0 for plasma renin activity (μg/l/h), active renin concentration (ng/l), Na (nmol/l), K (nmol/l), Cl (nmol/l), LH (IU/l), FSH (IU/l), alkaline phosphatase (IU/l) and PTHrP (pmol/l).
*Clinical findings before 3 years of age have been reported previously.[7]
†ACTH 0·25 mg bolus i.v.; blood sampling at 60 min.
‡Electrolyte values at the time of severe gastroenteritis; other biochemical data in reference to adrenal dysfunction were obtained after recovery from gastroenteritis and before glucocorticoid supplementation therapy.
§Reference age for Tanner stage 2 breast development in Japanese girls.[29]
¶Reference age for Tanner stage 4 pubic hair development in Japanese boys.[29]
**GnRH 100 $\mu g/m^2$ bolus i.v.; blood sampling at 0, 30, 60, 90, and 120 min.

Table 2. Summary of clinical features of cases 1–3

	Case 1	Case 2	Case 3
CDKN1C mutation	Yes	Yes	No
Previously reported IMAGe syndrome-compatible phenotype			
IUGR	Yes	Yes	Yes
Metaphyseal dysplasia	Yes	Yes	Yes
Adrenal hypoplasia	Yes*	Yes*	Yes*
Genital abnormality	(Female)	Yes	Yes
Hypercalciura†	Yes	No	Yes
Hitherto undescribed findings			
Body habitus	Relative macrocephaly	Relative macrocephaly	Relative macrocephaly
Skeletal			Arachnodactyly Lack of slender bones
Adrenal		FGD-like phenotype with no obvious mineralocorticoid deficiency	
Genital	Apparently normal pituitary-gonadal endocrine function	Apparently normal pituitary-gonadal endocrine function	Apparently normal pituitary-gonadal endocrine function
Others	Feeding difficulties	Feeding difficulties Oligohydramnios	

IUGR, intrauterine growth retardation; and FGD, familial glucocorticoid deficiency.
*Undetectable on magnetic resonance imaging and/or computed tomography.
†Frequent but not invariable feature.

pre- and postnatal body growth was severely impaired, pre- and postnatal OFC was relatively well preserved. In this regard, while *CDKN1C* is preferentially expressed from the maternal allele in most tissues, it is biparentally expressed at least in the foetal brain.[10] This expression pattern would be relevant to the relative macrocephaly in IMAGe syndrome. Notably, the combination of severely compromised body growth and well-preserved OFC is also characteristic of Silver–Russell syndrome (SRS) resulting

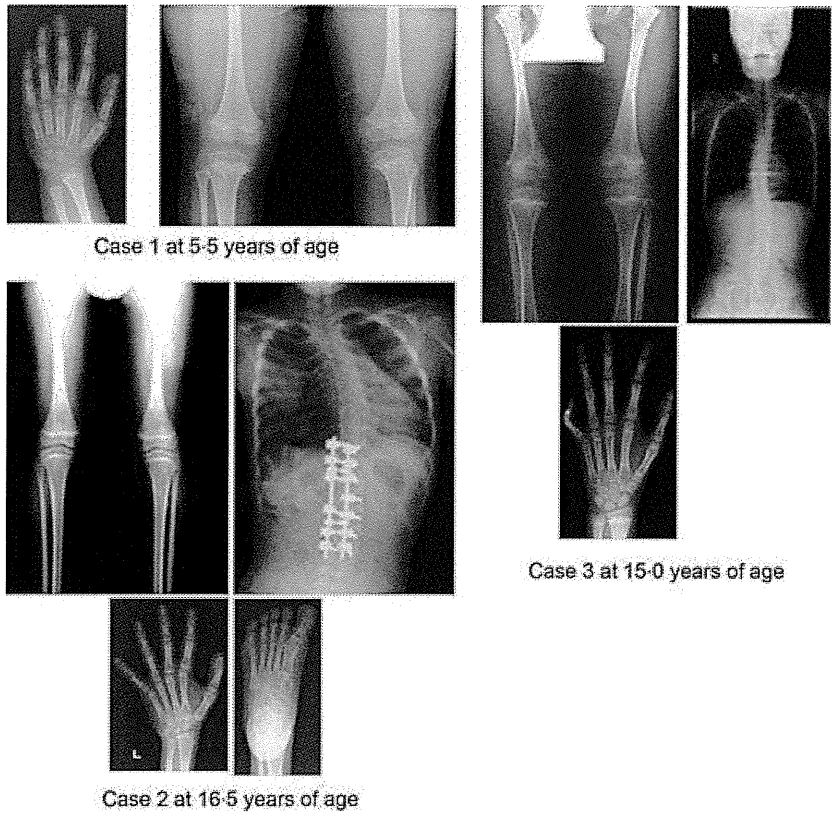

Fig. 2 Representative skeletal roentgenograms in cases 1–3.

from *H19*-DMR hypomethylation (epimutation),[11] and this is primarily consistent with paternal expression of the growth-promoting gene *IGF2* in the body and biparental expression of *IGF2* in the brain.[12] Thus, loss-of-imprinting in the brain tissue appears to underlie relative macrocephaly in both IMAGe syndrome and SRS.

Second, skeletal abnormalities including metaphyseal dysplasia were identified in cases 1 and 2. In this regard, skeletal phenotype of mice lacking *Cdkn1c* is grossly opposite of parathyroid hormone-related protein (PTHrP)-null phenotype,[13,14] and PTHrP permits skeletal development at least in part by suppressing *Cdkn1c* expression.[15] Thus, while serum calcium and calcium homeostasis-related factors were normal in cases 1 and 2, dysregulated PTHrP and/or PTH/PTHrP receptor signalling might be relevant to skeletal abnormalities in patients with gain-of-function mutations of *CDKN1C*. In addition, such a possible signalling defect might also be relevant to the frequent occurrence of hypercalciuria in IMAGe syndrome.

Third, adrenal dysfunction was mild in case 2, while case 1 experienced adrenal crisis in infancy as previously reported in patients with *CDKN1C* mutations.[1,3,4] Indeed, adrenal phenotype of case 2 is similar to that of patients with FGD rather than adrenal hypoplasia.[8,9] Our results therefore would expand the clinical spectrum of adrenal dysfunction in patients with *CDKN1C* mutations. For adrenal dysfunction, cortisol and aldosterone values remained within the normal range at the time of adrenal crisis in case 1 (Table 1). However, as adrenocorticotropic hormone and active renin concentrations were markedly increased, the overall results would be consistent with primary hypoadrenalism, as has been described previously.[16] This notion would also apply to the adrenal dysfunction in case 3 who had apparently normal aldosterone value and markedly increased plasma renin activity at the time of adrenal crisis.

Lastly, although male case 2 had bilateral cryptorchidism and small testes, pituitary-gonadal endocrine function was apparently normal as was secondary sexual development. Previously reported patients with *CDKN1C* mutations, as well as those who have not been examined for *CDKN1C* mutations, also have undermasculinized external genitalia in the presence of apparently normal endocrine function and pubertal development.[1–4,17,18] Notably, an episode of oligohydramnios was found in case 2 and has also been described in a 46,XY IMAGe syndrome patient with cryptorchidism.[19] This may imply the presence of placental hypoplasia and resultant chorionic gonadotropin deficiency as an underlying factor for genital anomalies.[11] In support of this notion, imprinted genes are known to play a pivotal role in body and placental growth,[20] and SRS is often associated with oligohydramnios, placental hypoplasia and undermasculinization.[11,21]

Genetic heterogeneity in IMAGe syndrome

Molecular data in case 3 imply the presence of genetic heterogeneity in IMAGe syndrome. Indeed, there was neither demonstrable *CDKN1C* mutation nor evidence for increased *CDKN1C* expression, while a pathologic mutation leading to gain-of-function or

increased expression of *CDKN1C* might reside on an unexamined region(s) such as promoter or enhancer sequences. In this regard, while case 3 showed IMAGe syndrome-compatible clinical features such as IUGR, metaphyseal dysplasia, adrenal hypoplasia and genital abnormalities, case 3 lacked slender bones and had arachnodactyly, in contrast to *CDKN1C*-mutation-positive cases 1 and 2. Such mild but discernible phenotypic variation might reflect the genetic heterogeneity. This matter might be clarified in the future by extensive studies such as exome or whole-genome sequencing. In particular, when such *CDKN1C*-mutation-negative patients with IMAGe syndrome-compatible phenotype have been accumulated, a novel gene(s) mutated in such patients may be identified. In this regard, if such a gene(s) exist, it is predicted to reside in the signal transduction pathway involving *CDKN1C*.

Relevance of CDKN1C mutations to atypical IMAGe syndrome and SRS

CDKN1C mutations have also been identified in atypical IMAGe syndrome and SRS (Fig. 1a). Hamajima *et al.* revealed a maternally inherited p.Ile272Ser mutation in three siblings (two males and one female) who manifested IUGR and adrenal insufficiency, and male genital abnormalities, but had no skeletal lesion.[22] Similarly, Brioude *et al.* found a maternally transmitted p.Arg279Leu mutation in six relatives (all females) from a four-generation family who satisfied the SRS diagnostic criteria,[23,24] after studying 97 SRS patients without known causes of SRS, that is, hypomethylation (epimutation) of the *H19*-DMR, duplication of the ICR2 and maternal uniparental disomy for chromosome 7 (upd(7)mat).[24] Notably, although both mutations had no significant effect on a cell cycle, they were associated with increased protein stability that appears to be consistent with the gain-of-function effects.[22,24] Such increased stability was also found for IMAGe-associated missense mutant proteins,[22] and an altered cell cycle with a significantly higher proportion of cells in the G1 phase was shown for an IMAGe-associated p.Arg279Pro mutation.[24] It is possible therefore that relatively severe *CDKN1C* gain-of-function effects lead to IMAGe syndrome and relatively mild *CDKN1C* gain-of-function effects result in SRS, with intermediate *CDKN1C* gain-of-function effects being associated with atypical IMAGe syndrome.[24]

Thus, it would not be surprising that cases 1–3 also met the SRS diagnostic criteria (Table 3).[23,24] Indeed, cases 1–3, as well as *CDKN1C*-mutation-positive SRS patients,[24] exhibited pre- and post-natal growth failure with relative macrocephaly and frequently manifested feeding difficulties and/or low body mass index (BMI) at two years of age. However, while relative macrocephaly is usually obvious at birth in SRS patients with *H19*-DMR epimutations and upd(7)mat,[21,23,25] it is more obvious at 2 years of age than at birth in *CDKN1C*-mutation-positive SRS patients.[24] Furthermore, *CDKN1C*-mutation-positive SRS patients are free from body asymmetry,[24] as are typical and atypical IMAGe syndrome patients described in this study and in the previous studies.[1–4,7,22] Thus, SRS caused by *CDKN1C* mutations may be characterized by clinically discernible macrocephaly at two years of age and lack of body asymmetry.

Table 3. Silver–Russell syndrome phenotypes in cases 1–3 and in affected relatives reported by Brioude *et al.*

	Case 1	Case 2	Case 3	Brioude *et al.**
Mandatory criteria				
IUGR†	Yes	Yes	Yes	4/4
Scoring system criteria				
Postnatal short stature (≤−2 SDS)	Yes	Yes	Yes	4/4
Relative macrocephaly‡	Yes	Yes	Yes	4/4§
Prominent forehead during early childhood	Yes	Yes	Yes	4/4
Body asymmetry	No	No	No	0/4
Feeding difficulties during early childhood and/or low BMI (<−2·0 SDS) around 2 years of age	Yes	Yes	Unknown	3/4 (1/4 & 2/4)¶

IUGR, Intrauterine growth retardation; SDS, standard deviation score; and BMI, body mass index.
The SRS diagnostic criteria proposed by Netchine *et al.*[23] and Brioude *et al.*[24] (low BMI around 2 years of age is included in Brioude *et al.*, but not in Netchine *et al.*): The diagnosis of SRS is made, when mandatory criteria plus at least three of the five scoring system criteria are observed. For detailed clinical features in cases 1–3, see Table 1.
*While six relatives were found to have *CDKN1C* mutation, detailed clinical features have been obtained in four mutation-positive relatives.[24]
†Birth length and/or birth weight ≤−2 SDS for gestational age.
‡SDS for birth length or birth weight minus SDS for birth occipitofrontal circumference ≤−1·5.
§Relative macrocephaly is more obvious at 2 years of age (4/4) than at birth (2/4).
¶One patient is positive for feeding difficulties, and other two patients are positive for low BMI.

Conclusion

In summary, we studied three patients with IMAGe syndrome. The results provide implications for phenotypic spectrum, underlying factor(s) in the development of each phenotype and genetic heterogeneity in IMAGe syndrome, as well as a phenotypic overlap between IMAGe syndrome and SRS. Further studies will permit to elucidate such matters.

Funding

This study was supported in part by Grants-in-Aid for Scientific Research (A) (25253023) and for Scientific Research on Innovative Areas (22132004-A01) from the Ministry of Education, Culture, Sports, Science and Technology, by Grant for Research on Intractable Diseases from the Ministry of Health, Labor and Welfare (H24-048), and by Grants from National Center for Child Health and Development (23A-1, 24-7 and 25-10).

Declaration of interest

The authors have nothing to declare.

References

1 Vilain, E., Le Merrer, M., Lecointre, C. *et al.* (1999) IMAGe, a new clinical association of intrauterine growth retardation, metaphyseal dysplasia, adrenal hypoplasia congenita, and genital anomalies. *Journal of Clinical Endocrinology and Metabolism*, **84**, 4335–4340.

2 Balasubramanian, M., Sprigg, A. & Johnson, D.S. (2010) IMAGe syndrome: case report with a previously unreported feature and review of published literature. *American Journal of Medical Genetics A*, **152A**, 3138–3142.

3 Bergadá, I., Del Rey, G., Lapunzina, P. *et al.* (2005) Familial occurrence of the IMAGe association: additional clinical variants and a proposed mode of inheritance. *Journal of Clinical Endocrinology and Metabolism*, **90**, 3186–3190.

4 Arboleda, V.A., Lee, H., Parnaik, R. *et al.* (2012) Mutations in the PCNA-binding domain of CDKN1C cause IMAGe syndrome. *Nature Genetics*, **44**, 788–792.

5 Demars, J. & Gicquel, C. (2012) Epigenetic and genetic disturbance of the imprinted 11p15 region in Beckwith-Wiedemann and Silver-Russell syndromes. *Clinical Genetics*, **81**, 350–361.

6 Lee, M.-H., Reynisdottir, I. & Massague, J. (1995) Cloning of p57(KIP2), a cyclin-dependent kinase inhibitor with unique domain structure and tissue distribution. *Genes and Development*, **9**, 639–649.

7 Amano, N., Naoaki, H., Ishii, T. *et al.* (2008) Radiological evolution in IMAGe association: a case report. *American Journal of Medical Genetics A*, **146A**, 2130–2133.

8 El-Khairi, R., Martinez-Aguayo, A., Ferraz-de-Souza, B. *et al.* (2011) Role of DAX-1 (NR0B1) and steroidogenic factor-1 (NR5A1) in human adrenal function. *Endocrine Development*, **20**, 38–46.

9 Meimaridou, E., Hughes, C.R., Kowalczyk, J. *et al.* (2013) Familial glucocorticoid deficiency: new genes and mechanisms. *Molecular and Cellular Endocrinology*, **371**, 195–200.

10 Matsuoka, S., Thompson, J.S., Edwards, M.C. *et al.* (1996) Imprinting of the gene encoding a human cyclin-dependent kinase inhibitor, p57KIP2, on chromosome 11p15. *Proceedings of the National Academy of Sciences of the USA*, **93**, 3026–3030.

11 Yamazawa, K., Kagami, M., Nagai, T. *et al.* (2008) Molecular and clinical findings and their correlations in Silver-Russell syndrome: implications for a positive role of IGF2 in growth determination and differential imprinting regulation of the IGF2-H19 domain in bodies and placentas. *Journal of Molecular Medicine*, **86**, 1171–1181.

12 Ulaner, G.A., Yang, Y., Hu, J.F. *et al.* (2003) CTCF binding at the insulin-like growth factor-II (IGF2)/H19 imprinting control region is insufficient to regulate IGF2/H19 expression in human tissues. *Endocrinology*, **144**, 4420–4426.

13 Zhang, P., Leigeois, N.J., Wong, C. *et al.* (1997) Altered cell differentiation and proliferation in mice lacking p57(KIP2) indicates a role in Beckwith-Wiedemann syndrome. *Nature*, **387**, 151–158.

14 Karaplis, A.C., Luz, A., Glowacki, J. *et al.* (1994) Lethal skeletal dysplasia from targeted disruption of the parathyroid hormone-related peptide gene. *Genes & Development*, **8**, 277–289.

15 MacLean, H.E., Guo, J., Knight, M.C. *et al.* (2004) The cyclin-dependent kinase inhibitor p57(Kip2) mediates proliferative actions of PTHrP in chondrocytes. *Journal of Clinical Investigation*, **113**, 1334–1343.

16 Stewart, P.M. & Krone, N.P. (2011) The adrenal cortex. In: S. Melmed, K.S. Polonsky, P.R. Larsen, H.N. Kronenberg eds. Williams Textbook of Endocrinology, 12th edn. Elsevier, Saunders, 479–577.

17 Lienhardt, A., Mas, J.C., Kalifa, G. *et al.* (2002) IMAGe association: additional clinical features and evidence for recessive autosomal inheritance. *Hormone Research*, **57**(Suppl 2), 71–78.

18 Pedreira, C.C., Savarirayan, R. & Zacharin, M.R. (2004) IMAGe syndrome: a complex disorder affecting growth, adrenal and gonadal function, and skeletal development. *Journal of Pediatrics*, **144**, 274–277.

19 Ko, J.M., Lee, J.H., Kim, G.H. *et al.* (2007) A case of a Korean newborn with IMAGe association presenting with hyperpigmented skin at birth. *European Journal of Pediatrics*, **166**, 879–880.

20 Fowden, A.L., Sibley, C., Reik, W. *et al.* (2006) Imprinted genes, placental development and fetal growth. *Hormone Research*, **65** (Suppl 3), 50–58.

21 Wakeling, E.L., Amero, S.A., Alders, M. *et al.* (2010) Epigenotype-phenotype correlations in Silver-Russell syndrome. *Journal of Medical Genetics*, **47**, 760–768.

22 Hamajima, N., Johmura, Y., Suzuki, S. *et al.* (2013) Increased protein stability of CDKN1C causes a gain-of-function phenotype in patients with IMAGe syndrome. *PLoS ONE*, **8**, e75137.

23 Netchine, I., Rossignol, S., Dufourg, M.N. *et al.* (2007) 11p15 imprinting center region 1 loss of methylation is a common and specific cause of typical Russell-Silver syndrome: clinical scoring system and epigenetic-phenotypic correlations. *Journal of Clinical Endocrinology and Metabolism*, **92**, 3148–3154.

24 Brioude, F., Oliver-Petit, I., Blaise, A. *et al.* (2013) CDKN1C mutation affecting the PCNA-binding domain as a cause of familial Russell Silver syndrome. *Journal of Medical Genetics*, **50**, 823–830.

25 Fuke, T., Mizuno, S., Nagai, T. *et al.* (2013) Molecular and clinical studies in 138 Japanese patients with Silver-Russell syndrome. *PLoS ONE*, **8**, e60105.

26 Suwa, S., Tachibana, K., Maesaka, H. *et al.* (1992) Longitudinal standards for height and height velocity for Japanese children from birth to maturity. *Clinical Pediatric Endocrinology*, **1**, 5–14.

27 Inokuchi, M., Matsuo, N., Anzo, M. *et al.* (2007) Body mass index reference values (mean and SD) for Japanese children. *Acta Paediatrica*, **96**, 1674–1676.

28 Japan Public Health Association. (1996) Normal Biochemical Values in Japanese Children. Sanko Press, Tokyo, (in Japanese).

29 Matsuo, N. (1993) Skeletal and sexual maturation in Japanese children. *Clinical Pediatric Endocrinology*, **2**(Suppl), 1–4.

Supporting Information

Additional Supporting Information may be found in the online version of this article:

Table S1. Primers utilized in this study.

Paris, Februrary 7 th 2015

Dear Colleague,

On behalf of the organising committee of our COST European Network for human congenital imprinting disorders (EUCID, http://www.imprinting-disorders.eu), we would like to invite you to participate in a consensus meeting on Silver-Russell syndrome, in Barcelona, following the ESPE meeting, in october 2015 (Arrival on the October 3 rd in the evening, 4rd-5th for all the participants and 6 th for the chairs and secretaries of each working group).

Silver-Russell Syndrome/Russell-Silver Syndrome, has been described in 1953-1954. Since then, many cases have been published in the litterature, however the clinical and molecular diagnoses remain difficult, the prevalence is unknown and no published specific clinical guidelines are available.

A consensus on clinical, molecular diagnoses and care guidelines in keeping with evidence based publication and with the experience of experts, is needed for this group of patients as well as for research in this field.

As an expert in the field, we would be very happy if you agree to participate. If you do not intend to attend the ESPE meeting, your travel expenses to Barcelona, including hotel, will be covered by COST (following the COST rules of reimbursement). If you are attending the ESPE meeting, the additional nights of hotel and meals during the consensus meeting will be covered by COST. We will have 3 different work groups (WG1: Clinical diagnosis; WG2: Molecular diagnosis; WG2: Clinical guidelines) with common and separate working sessions. All participants will contribute to a synthesis of this work. Prior to the meeting, a detailed methodology as well as a consensus chart will be sent to you. If you agree to participate, your attendance during the entire meeting is required in order to build a consensus.

Please let us know as soon as possible if you can attend this consensus meeting, as the number of participants is limited due to funding constraints and to allow for fruitful discussion.

With Best regards,

Irène Netchine, Karen Temple & Thomas Eggermann, on Behalf of the COST organising committee for SRS/RSS consensus.

EUCID.net
European network of Congenital Imprinting Disorders

EJHG Open

European Journal of Human Genetics (2015), 1–11

www.nature.com/ejhg

ARTICLE

Comprehensive clinical studies in 34 patients with molecularly defined UPD(14)pat and related conditions (Kagami–Ogata syndrome)

Masayo Kagami[1], Kenji Kurosawa[2], Osamu Miyazaki[3], Fumitoshi Ishino[4], Kentaro Matsuoka[5] and Tsutomu Ogata*[,1,6]

Paternal uniparental disomy 14 (UPD(14)pat) and epimutations and microdeletions affecting the maternally derived 14q32.2 imprinted region lead to a unique constellation of clinical features such as facial abnormalities, small bell-shaped thorax with a coat-hanger appearance of the ribs, abdominal wall defects, placentomegaly, and polyhydramnios. In this study, we performed comprehensive clinical studies in patients with UPD(14)pat ($n=23$), epimutations ($n=5$), and microdeletions ($n=6$), and revealed several notable findings. First, a unique facial appearance with full cheeks and a protruding philtrum and distinctive chest roentgenograms with increased coat-hanger angles to the ribs constituted the pathognomonic features from infancy through childhood. Second, birth size was well preserved, with a median birth length of ±0 SD (range, −1.7 to +3.0 SD) and a median birth weight of +2.3 SD (range, +0.1 to +8.8 SD). Third, developmental delay and/or intellectual disability was invariably present, with a median developmental/intellectual quotient of 55 (range, 29–70). Fourth, hepatoblastoma was identified in three infantile patients (8.8%), and histological examination in two patients showed a poorly differentiated embryonal hepatoblastoma with focal macrotrabecular lesions and well-differentiated hepatoblastoma, respectively. These findings suggest the necessity of an adequate support for developmental delay and periodical screening for hepatoblastoma in the affected patients, and some phenotypic overlap between UPD(14)pat and related conditions and Beckwith–Wiedemann syndrome. On the basis of our previous and present studies that have made a significant contribution to the clarification of underlying (epi)genetic factors and the definition of clinical findings, we propose the name 'Kagami–Ogata syndrome' for UPD(14)pat and related conditions.
European Journal of Human Genetics (2015) **00**, 1–11. doi:10.1038/ejhg.2015.13

INTRODUCTION

Human chromosome 14q32.2 carries a cluster of imprinted genes including paternally expressed genes (*PEGs*) such as *DLK1* and *RTL1*, and maternally expressed genes (*MEGs*) such as *MEG3* (alias, *GTL2*), *RTL1as* (*RTL1* antisense), *MEG8*, *snoRNAs*, and *microRNAs* (Supplementary Figure S1).[1,2] The parental origin-dependent expression patterns are regulated by the germline-derived primary *DLK1-MEG3* intergenic differentially methylated region (IG-DMR) and the postfertilization-derived secondary *MEG3*-DMR.[2,3] Both DMRs are hypermethylated after paternal transmission and hypomethylated after maternal transmission in the body; in the placenta, the IG-DMR alone remains as a DMR with the same methylation pattern in the body, while the *MEG3*-DMR does not represent a differentially methylated pattern.[2,3] Consistent with such methylation patterns, the hypomethylated IG-DMR and *MEG3*-DMR of maternal origin function as imprinting control centers in the placenta and the body, respectively, and the IG-DMR behaves hierarchically as an upstream regulator for the methylation pattern of the *MEG3*-DMR in the body, but not in the placenta.[3,4]

Paternal uniparental disomy 14 (UPD(14)pat) (OMIM #608149) results in a unique constellation of clinical features such as facial abnormalities, small bell-shaped thorax with coat-hanger appearance of the ribs, abdominal wall defects, placentomegaly, and polyhydramnios.[2,5] These clinical features are also caused by epimutations (hypermethylations) and microdeletions affecting the maternally derived IG-DMR and/or *MEG3*-DMR (Supplementary Figure S1). Such UPD(14)pat and related conditions are rare, with reports of 33 patients with UPD(14)pat, five patients with epimutations, and nine patients with microdeletions (and four new UPD(14)pat patients reported here) (see Supplementary Table S1 for the reference list). For microdeletions, loss of the maternally inherited *MEG3*-DMR alone leads to a typical UPD(14)pat body phenotype and apparently normal placental phenotype,[3,4] whereas loss of the maternally derived IG-DMR alone or both DMRs results in a typical body and placental UPD(14)pat phenotype, consistent with the methylation patterns of the two DMRs.[2,3] Furthermore, correlations between clinical features and deleted segments have indicated the critical role of excessive *RTL1* (but not *DLK1*) expression in phenotypic development.[2,6] Such an excessive *RTL1* expression is primarily due to loss of functional *RTL1as*-encoded *microRNAs* that act as a *trans*-acting repressor for *RTL1* expression.[6] Indeed, the *RTL1* expression level is ~5 times, rather than 2 times, increased in placentas with UPD(14)pat

[1]Department of Molecular Endocrinology, National Research Institute for Child Health and Development, Tokyo, Japan; [2]Division of Medical Genetics, Kanagawa Children's Medical Center, Yokohama, Japan; [3]Department of Radiology, National Center for Child Health and Development, Tokyo, Japan; [4]Department of Epigenetics, Medical Research Institute, Tokyo Medical and Dental University, Tokyo, Japan; [5]Department of Pathology, National Center for Child Health and Development, Tokyo, Japan; [6]Department of Pediatrics, Hamamatsu University School of Medicine, Hamamatsu, Japan

*Correspondence: Dr T Ogata, Department of Pediatrics, Hamamatsu University School of Medicine, Hamamatsu 431-3192, Japan. Tel: +81 53 435 2310; Fax: +81 53 435 2310; E-mail: tomogata@hama-med.ac.jp

Received 30 August 2014; revised 7 January 2015; accepted 14 January 2015

Table 1 Clinical manifestations in 33 Japanese and one Irish patients with UPD(14)pat and related conditions (Kagami–Ogata syndrome)

	UPD(14)pat	*Epimutations*	*Microdeletions*				*Total*
			Subtype 1	*Subtype 2*	*Subtype 3*	*Subtotal*	
	Pts 1–23 (n = 23)	*Pts 24–28 (n = 5)*	*Pts 29–31 (n = 3)*	*Pt 32 (n = 1)*	*Pts 33–34 (n = 2)*	*Pts 29–34 (n = 6)*	*Pts 1–34 (n = 34)*
Age at the last examination or death (y)	2.9 (0.0–15.0)	2.0 (0.8–5.5)	2.8 (0.8–8.9)	(4 days)	4.5 (3.8–5.1)	3.3 (0.0–8.9)	2.8 (0.0–15.0)
Sex (male:female)	9:14	3:2	1:2	0:1	0:2	1:5	13:21
Molecular findings[a]							
IG-DMR of maternal origin	Absent	Methylated	Deleted	Unmethylated	Deleted		
MEG3-DMR of maternal origin	Absent	Methylated[b]	Deleted/methylated[b]	Deleted	Deleted		
DLK1 expression level	2×	2×	1 or 2×	2× (1×)[c]	1 or 2×		
RTL1 expression level	~5×	~5×	~5×	~5× (1× or ~2.5×)[c]	~2.5×		
MEGs expression level	0×	0×	0×	0× (1× or 0×)[c]	0×		
Pregnancy and delivery							
Polyhydramnios	23/23	5/5	3/3	0/1	2/2	5/6	33/34
Gestational age at Dx (w)	25 (14–30)	27.5 (22–30)	Unknown	—	21	21	25.5 (14–30)
Amnioreduction	18/20	4/5	2/3	0/1	1/2	3/6	25/31
Amnioreduction (>30 w)	18/18	4/4	2/2	—	1/1	3/3	25/25[d]
Placentomegaly[e]	14/17	4/4	3/3	0/1	2/2	5/6	23/27
Prenatal Dx of thoracic abnormality	8/20[f]	2/3	0/1	—	0/1	0/2	10/25
Gestational age at Dx (w)	26 (22–33)	27.5 (25–30)	—	—	—	—	26 (22–33)
Prenatal Dx of abdominal abnormality	6/18	3/3	1/1	—	0/1	1/2	10/23
Gestational age at Dx (w)	26 (22–28)	25	Unknown	Unknown	Unknown	Unknown	25.5 (22–28)
Gestational age (w)	34.5 (24–38)	35 (30–37)	30 (27–33)	28	32.5 (30–35)	30 (27–35)	34 (24–38)
Premature delivery (<37 w)	17/23	4/5	3/3	1/1	2/2	6/6	27/34
Delivery (Cesarean:Vaginal)	15:8	4:1	2:1	0:1	2:0	4:2	23:11
Medically assisted reproduction	1/18	0/1	0/1	Unknown	0/1	0/2	1/21
Growth pattern							
Prenatal growth failure[g]	0/23	0/5	0/3	0/1	0/2	0/6	0/34
Prenatal overgrowth[h]	13/23	3/5	3/3	0/1	1/2	4/6	20/34
Birth length (patient number)	21	5	1	1	2	4	30
SD score, median (range)	+0.3 (–1.7 to +3.0)	–0.5 (–0.9 to +1.4)	0.0	–1.1	+0.7 (–0.1 to +1.5)	–0.1 (–1.1 to +1.5)	±0 (–1.7 to +3.0)
Actual length (cm), median (range)	45.0 (30.6 to 51.0)	43.5 (41.0 to 50.0)	43.0	34.0	43.5 (42.0 to 45.0)	42.5 (34.0 to 45.0)	44.7 (30.6 to 51.0)
Birth weight (patient number)	23	5	3	1	2	6	34
SD score, median (range)	+2.2 (+0.1 +8.8)	+2.2 (+0.5 to +3.7)	+2.8 (+2.4 to +3.7)	+1.5	+1.7 (+0.9 to +2.5)	+2.5 (+0.9 to +3.7)	+2.3 (+0.1 to +8.8)
Actual weight (cm), median (range)	2.79 (1.24 to 3.77)	2.9 (1.61 to 3.28)	2.04 (1.30 to 2.84)	1.32	2.24 (1.55 to 2.94)	1.79 (1.30 to 2.94)	2.79 (1.24 to 3.77)
Postnatal growth failure[i]	7/20	2/5	2/3	—	0/2	2/5	11/30
Postnatal overgrowth[j]	1/20	1/5	0/3	—	0/2	0/5	2/30
Present stature (patient number)	20	5	3	—	1	4	29
SD score, median (range)	–1.6 (–8.7 to +1.1)	–1.8 (–7.1 to +0.9)	–2.2 (–3.3 to –1.3)	—	–1.6	–1.9 (–3.3 to –1.3)	–1.6 (–8.7 to +1.1)
Present weight (patient number)	20	5	3	—	2	5	30
SD score, median (range)	–1.0 (–6.0 to +2.4)	–0.6 (–5.5 to +4.0)	–1.3 (–2.2 to ±0)	—	–1.1 (–1.3 to –0.9)	–1.3 (–2.2 to ±0)	–1.0 (–6.0 to +4.0)

Table 1 (Continued)

	UPD(14)pat	*Epimutations*	*Microdeletions*				*Total*
			Subtype 1	*Subtype 2*	*Subtype 3*	*Subtotal*	
	Pts 1–23 (n = 23)	*Pts 24–28 (n = 5)*	*Pts 29–31 (n = 3)*	*Pt 32 (n = 1)*	*Pts 33–34 (n = 2)*	*Pts 29–34 (n = 6)*	*Pts 1–34 (n = 34)*
Craniofaciocervical features							
Frontal bossing	17/22	4/5	1/3	1/1	2/2	4/6	25/33
Hairy forehead	18/22	1/5	3/3	1/1	0/2	4/6	23/33
Blepharophimosis	18/22	3/5	2/3	0/1	1/2	3/6	24/33
Small ears	8/21	2/5	1/3	1/1	0/2	2/6	12/32
Depressed nasal bridge	23/23	5/5	3/3	0/1	1/2	4/6	32/34
Anteverted nares	19/22	4/5	3/3	0/1	2/2	5/6	28/33
Full cheek	20/21	4/4	2/2	0/1	1/1	3/4	27/29
Protruding philtrum	23/23	5/5	3/3	0/1	2/2	5/6	33/34
Puckered lips	11/21	3/5	3/3	0/1	0/2	3/6	17/32
Micrognathia	20/21	5/5	3/3	1/1	1/2	5/6	30/32
Short webbed neck	22/22	5/5	3/3	1/1	2/2	6/6	33/33
Thoracic abnormality							
Small bell-shaped thorax in infancy[k]	23/23	5/5	3/3	1/1	2/2	6/6	34/34
Coat-hanger appearance in infancy[l]	23/23	5/5	3/3	1/1	2/2	6/6	34/34
Laryngomalacia	8/20	2/5	2/3	—	0/1	2/4	12/29
Tracheostomy	7/21	1/4	0/2	—	2/2	2/4	10/29
Mechanical ventilation	21/23	5/5	3/3	1/1	2/2	6/6	32/34
Duration of ventilation (m)[m]	1.2 (0.1–17)	0.7 (0.1–0.9)	5 (0.23–10)	—	1.5 (1–2)	2 (0.2–10)	1.0 (0.1–17)
Abdominal wall defects							
Omphalocele	7/23	2/5	1/3	1/1	0/2	2/6	11/34
Diastasis recti	16/23	3/5	2/3	0/1	2/2	4/6	23/34
Developmental delay							
Developmental delay	21/21	5/5	3/3	—	2/2	5/5	31/31
Developmental/intellectual quotient	55 (29–70)	52 (48–56)	Unknown	Unknown	Unknown	—	55 (29–70)
Delayed head control (>4 m)[n]	14/16	4/4	1/1	—	1/1	2/2	20/22
Age at head control (m)[o]	7 (3–36)	7 (6–11)	6	—	6	6 (6)	7 (3–36)
Delayed sitting without support (>7 m)[n]	16/16	4/4	2/2	—	1/1	3/3	23/23
Age at sitting without support (m)[o]	12 (8–25)	11.5 (10–20)	22.5 (18–27)	—	18	18 (18–27)	12 (8–27)
Delayed walking without support (>14 m)[n]	17/17	3/3	2/2	—	2/2	4/4	24/24
Age at walking without support (m)[o]	25.5 (20–49)	25 (22–39)	60 (30–90)	—	24	30 (24–90)	25.5 (20–90)
Other features							
Feeding difficulty	20/21	5/5	3/3	—	2/2	5/5	30/31
Duration of tube feeding (m)[p]	6 (0.1–72)	8.5 (0.5–17)	59.5 (30–89)	—	51	51 (30–89)	7.5 (0.1–89)
Joint contractures	14/22	3/5	3/3	0/1	0/2	3/6	20/33
Constipation	12/20	3/4	1/2	—	0/2	1/4	16/28
Kyphoscoliosis	9/21	3/5	1/2	0/1	0/1	1/4	13/30

Table 1 (Continued)

	UPD(14)pat	*Epimutations*	*Microdeletions*				*Total*
			Subtype 1	*Subtype 2*	*Subtype 3*	*Subtotal*	
	Pts 1–23 (n = 23)	*Pts 24–28 (n = 5)*	*Pts 29–31 (n = 3)*	*Pt 32 (n = 1)*	*Pts 33–34 (n = 2)*	*Pts 29–34 (n = 6)*	*Pts 1–34 (n = 34)*
Coxa valga	6/21	1/5	3/3	0/1	1/2	4/6	11/32
Cardiac disease	5/22	1/5	0/3	1/1	1/2	2/6	8/33
Inguinal hernia	5/22	1/5	2/3	0/1	0/2	2/6	8/33
Seizure	1/21	0/5	0/3	0/1	0/2	0/6	1/32
Hepatoblastoma	3/23	0/5	0/3	0/1	0/2	0/6	3/34
Mortality within the first 5 years							
Alive:deceased	18:5	5:0	2:1	0:1	1:1	3:3	26:8
Parents							
Paternal age at childbirth (y)	35 (24–47)	30 (26–36)	37 (34–39)	25	31.5 (27–36)	35 (25–39)	34 (24–47)
Maternal age at childbirth (y)	31 (25–43)	28 (25–35)	31 (27–36)	25	30.5 (28–33)	29.5 (25–36)	31 (25–43)
Advanced childbearing age (⩾35 y)	8/23	1/5	1/3	0/1	0/2	1/6	8/34

Abbreviations: CHA, coat-hanger angle; Dx, diagnosis; m, month; M/W, mid to widest thorax diameter; UPD(14), uniparental disomy 14; w, week; y, year.
Patient #32 is Irish, and the remaining patients are Japanese; the Irish patient has also been examined by Beygo *et al.*[4]
Age data are expressed by median and range.
The denominators indicate the number of patients examined for the presence or absence of each feature, and the numerators represent the number of patient assessed to be positive for that feature; thus, differences between the denominators and numeratorsdenote the number of patients evaluated to be negative for the feature.
[a]For details, see Supplementary Figures S1 and S2.
[b]The *MEG3*-DMR is predicted to be grossly hypomethylated in the placenta.
[c]Expression patterns of the imprinted genes are predicted to be different between the body and the placenta in this patient, while they are predicted to be identical between the body and the placenta in other patients (See Supplementary Figure S1).
[d]Amnioreduction was performed about two times in 23 of the 25 pregnancies.
[e]Placental weight >120% of the gestational age-matched mean placental weight.[34]
[f]The diagnosis of UPD(14)pat has been suspected in two patients (patients #7 and #21).
[g]Birth length and/or birth weight <−2 SD of the gestational age- and sex-matched Japanese reference data (http://jspe.umin.jp/medical/keisan.html).
[h]Birth length and/or birth weight >+2 SD of the gestational age- and sex-matched Japanese reference data (http://jspe.umin.jp/medical/keisan.html).
[i]Present length/height and/or present weight <−2 SD of the age- and sex-matched Japanese reference data (http://jspe.umin.jp/medical/taikaku.html).
[j]Present length/height and/or present weight >+2 SD of the age- and sex-matched Japanese reference data (http://jspe.umin.jp/medical/taikaku.html).
[k]The M/W ratio below nromal range (see Figure 2).
[l]The CHA above the normal range (see Figure 2).
[m]The duration in patients in whom mechanical ventilation could be discontinued.
[n]The age when 90% of infants pass each gross motor developmental milestone (based on Revised Japanese Version of Denver Developmental Screening Test) (http://www.dinf.ne.jp/doc/japanese/prdl/jsrd/norma/n175/img/n175_078i01.gif).
[o]The median (range) of ages in patients who passed each gross motor developmental milestone; patients who have not passed each milestone are not included.
[p]The duration in patients in whom tube feeding could be discontinued.

accompanied by two copies of functional *RTL1* and no functional *RTL1as*.[6] This implies that the *RTL1* expression level is ~2.5 times increased in the absence of functional *RTL1as*-encoded *microRNAs*.

Here, we report comprehensive clinical findings in a series of patients with molecularly confirmed UPD(14)pat and related conditions, and suggest pathognomonic and/or characteristic features and their underlying factors. We also propose the name 'Kagami–Ogata syndrome' for UPD(14)pat and related conditions.

MATERIALS AND METHODS

Ethical approval

This study was approved by the Institute Review Board Committee at the National Center for Child Health and Development, and performed after obtaining written informed consent to publish the clinical and molecular information. We also obtained written informed consent with parental signature to publish facial photographs.

Patients

This study consisted of 33 Japanese patients and one Irish patient (patient #32) with UPD(14)pat and related conditions (13 males and 21 females; 31 patients with normal karyotypes and two patients (#17 and #20) with Robertsonian translocations involving chromosome 14 (karyotyping not performed in patient #1); 30 previously described patients[2,3,7–10] and four new patients) in whom underlying (epi)genetic causes were clarified and detailed clinical findings were obtained (Supplementary Table S2).

The 34 patients were classified into three groups according to the underlying (epi)genetic causes that were determined by methylation analysis for the two DMRs, microsatellite analysis for a total of 24 loci widely dispersed on chromosome 14, fluorescence *in situ* hybridization for the two DMRs, and oligonucleotide array-based comparative genomic hybridization for the 14q32.2 imprinted region, as reported previously:[9] (1) 23 patients with UPD(14)pat (UPD-group); (2) five patients with epimutations (Epi-group); and (3) six patients with microdeletions (Del-group) (Supplementary Figure S2).

Furthermore, the 23 patients of UPD-group were divided into three subtypes in terms of UPD generation mechanisms by microsatellite analysis, as reported previously:[9] (1) 13 patients with monosomy rescue (MR) or postfertilization mitotic error (PE)-mediated UPD(14)pat indicated by full isodisomy (subtype 1) (UPD-S1); (2) a single patient with PE-mediated UPD(14)pat demonstrated by segmental isodisomy (subtype 2) (UPD-S2); and (3) nine patients with trisomy rescue (TR) or gamete complementation (GC)-mediated UPD(14)pat revealed by heterodisomy for at least one locus (subtype 3) (UPD-S3) (Supplementary Figure S2) (it is possible that some patients classified as UPD-S1 may have a cryptic heterodisomic region(s) and actually belong to UPD-S3). Similarly, the six patients of Del-group were divided into three subtypes in terms of the measured/predicted *RTL1* expression level in the body and placenta:[2,3] (1) three patients with ~5 times *RTL1* expression level in both the body and placenta (subtype 1) (Del-S1); (2) a single patient with about five times *RTL1* expression level in the body and normal (1 time) or ~2.5 times *RTL1* expression level in the placenta (subtype 2) (Del-S2); and (3) two patients with ~2.5 times *RTL1* expression level in both the body and placenta (subtype 3) (Del-S3) (Supplementary Figure S2). The measured/predicted expression patterns of the imprinted genes in each group/subtype are illustrated in Supplementary Figure S1.

Clinical studies

We used a comprehensive questionnaire to collect detailed clinical data of all patients from attending physicians. To evaluate chest roentgenographic findings, we obtained the coat-hanger angle (CHA) to the ribs and the ratio of the mid to widest thorax diameter (M/W ratio), as reported previously.[11] We also asked the physicians to report any clinical findings not covered by the questionnaire.

Statistical analysis

Statistical significance of the median among three groups and between two groups/subtypes was examined by the Kruskal–Wallis test and the Mann–Whitney's *U*-test, respectively, and that of the frequency among three groups and between two groups was analyzed by the Fisher's exact probability test, using the R environment (http://cran.r-project.org/bin/windows/base/old/2.15.1/). $P<0.05$ was considered significant. Kaplan–Meier survival curves were constructed using the R environment.

RESULTS

Clinical findings of each group/subtype are summarized in Table 1, and those of each patient are shown in Supplementary Table S2. Phenotypic findings were comparable among UPD-S1, UPD-S2, and UPD-S3, and somewhat different among Del-S1, Del-S2, and Del-S3, as predicted from the expression patterns of the imprinted genes (Supplementary Figure S1). Thus, we showed the data of UPD-group (the sum of UPD-S1, UPD-S2, and UPD-S3) and those of each subtype of Del-group (Del-S1, Del-S2, and Del-S3) in Table 1, and described the data of UPD-S1, UPD-S2, and UPD-S3 in Supplementary Table S3.

We registered the clinical information of each patient in the Leiden Open Variation Database (LOVD) (http://www.lovd.nl/3.0/home; http://databases.lovd.nl/shared/individuals), and the details of each microdeletion in the ClinVar Database (http://www.ncbi.nlm.nih.gov/clinvar/). The LOVD Individual IDs and the ClinVar SCV accession numbers are shown in Supplementary Table S2.

Pregnancy and delivery

Polyhydramnios was observed from ~25 weeks of gestation during the pregnancies of all patients, except for patient #32 of Del-S2 who had deletion of the *MEG3*-DMR and three of the seven *MEG3* exons, and usually required repeated amnioreduction, especially after 30 weeks of gestation. Placentomegaly was usually identified in patients affected with polyhydramnios, but not found in three patients of UPD-group. Thoracic and abdominal abnormalities were found by ultrasound studies in ~40% of patients from ~25 weeks of gestation, and UPD(14)pat was suspected in patients #7 and #21, due to delineation of the bell-shaped thorax with coat-hanger appearance of the ribs. Premature delivery was frequently observed, especially in Del-group. Because of fetal distress and polyhydramnios, ⩾two-thirds of the patients in each group were delivered by Cesarean section. Medically assisted reproduction was reported only in one (patient #8) of 21 patients for whom clinical records on conception were available.

Growth pattern

Prenatal growth was characterized by grossly normal birth length and obviously excessive birth weight. Indeed, birth length ranged from 30.6 to 51.0 cm (−1.7 to +3.0 SD for the gestational age- and sex-matched Japanese reference data) with a median of 44.7 cm (±0 SD), and birth weight ranged from 1.24 to 3.77 kg (+0.1 to +8.8 SD) with a median of 2.79 kg (+2.3 SD). Although birth weight was disproportionately greater than birth length, there was no generalized edema as a possible cause of overweight.

In contrast, postnatal growth was rather compromised, and growth failure (present length/height and/or weight < -2 SD) was observed in about one-third of patients of each group. Postnatal weight was better preserved than postnatal length/height.

Craniofaciocervical features

All patients exhibited strikingly similar craniofaciocervical features (Figure 1). Indeed, >90% of patients had depressed nasal bridge, full cheeks, protruding philtrum, micrognathia, and short webbed neck. In particular, the facial features with full cheeks and protruding philtrum

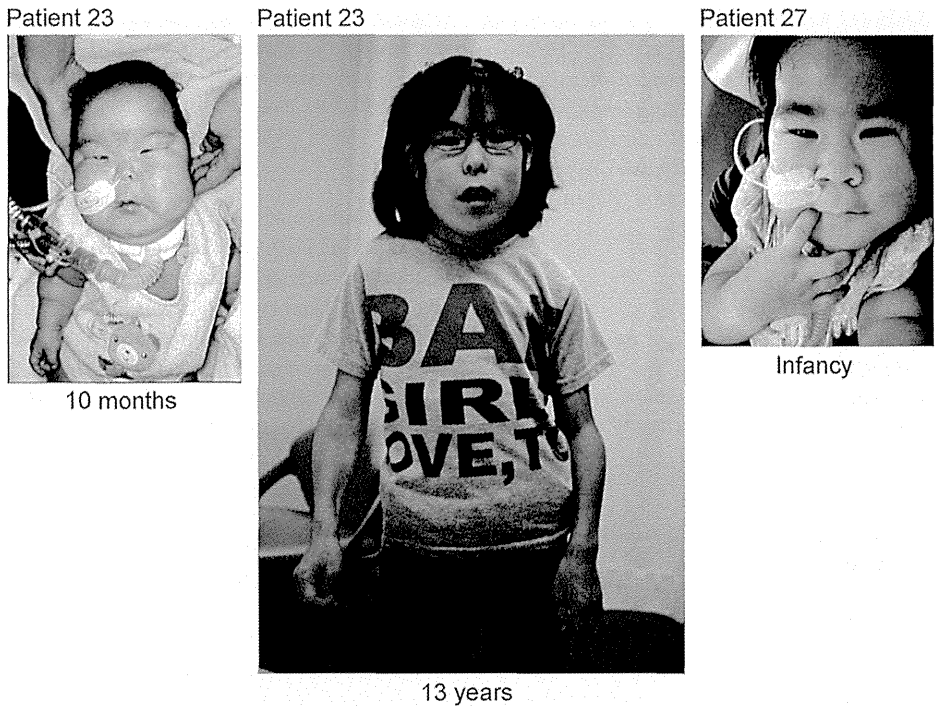

Figure 1 Photographs of patient #23 with UPD(14)pat and patient #27 with epimutation.

appeared to be specific to UPD(14)pat and related conditions, and were recognizable from infancy through childhood.

Thoracic abnormality

The 34 patients invariably showed small bell-shaped small thorax with coat-hanger appearance of the ribs in infancy (Figure 2). Long-term (≥10 years) follow-up in patient #12 of UPD-group and patient #31 of Del-S1 who had ~5 times of *RTL1* expression, and in patient #34 of Del-S3 who had ~2.5 times of *RTL1* expression, showed that the CHAs remained above the normal range of age-matched control children, while the M/W ratios, though they were below the normal range in infancy, became within the normal range after infancy (Figure 2). Laryngomalacia was also often detected in each group.

Mechanical ventilation was performed in all patients except for patients #14 and #20 of UPD-group, and tracheostomy was also carried out in about one-third of patients. Mechanical ventilation could be discontinued during infancy in 22 patients (Supplementary Figure S3). Ventilation duration was variable with a median period of 1 month among the 22 patients, and was apparently unrelated to the underlying genetic cause or gestational age.

Abdominal wall defects

Omphalocele was identified in about one-third of patients, and diastasis recti was found in the remaining patients.

Developmental status

Developmental delay (DD) and/or intellectual disability (ID) was invariably present in 26 patients examined (age, 10 months to 15 years), with the median developmental/intellectual quotient (DQ/IQ) of 55 (range, 29–70) (Figure 3). Gross motor development was also almost invariably delayed, with grossly similar patterns among different groups. In patients who passed gross motor developmental milestones, head control was achieved at ~7 months, sitting without support at ~12 months, and walking without support at ~2.1 years of age.

Other features

Several prevalent features were also identified. In particular, except for patient #22, feeding difficulty with poor sucking and swallowing was exhibited by all patients who were affected with polyhydramnios, and gastric tube feeding was performed in all patients who survived more than 1 week (Supplementary Figure S4). Tube-feeding duration was variable with a median period of ~7.5 months in 16 patients for whom tube feeding was discontinued, and tended to be longer in Del-group. In addition, there were several features manifested by single patients (Supplementary Table S2).

Notably, hepatoblastoma was identified at 46 days of age in patient #17, at 218 days in patient #18, and at 13 months of age in patient #8 of UPD-group (Figure 4). It was surgically removed in patients #8 and #18, although chemotherapy was not performed because of poor body condition. In patient #17, neither an operation nor chemotherapy could be carried out because of the patient's severely poor body condition. Histological examination of the removed tumors revealed a poorly differentiated embryonal hepatoblastoma with focal macrotrabecular lesions in patient #8 (Figure 4) and a well-differentiated hepatoblastoma in patient #18.[10]

Mortality

Eight patients were deceased before 4 years of age. The survival rate was 78% in UPD-group, 100% in Epi-group, and 50% in Del-group; it was 25% in patients born ≤29 weeks of gestation, 83% in those born 30–36 weeks of gestation, and 86% in those born ≥37 weeks of gestation (Figure 5). The cause of death was variable; however, respiratory problems were a major factor, because patient #1 died

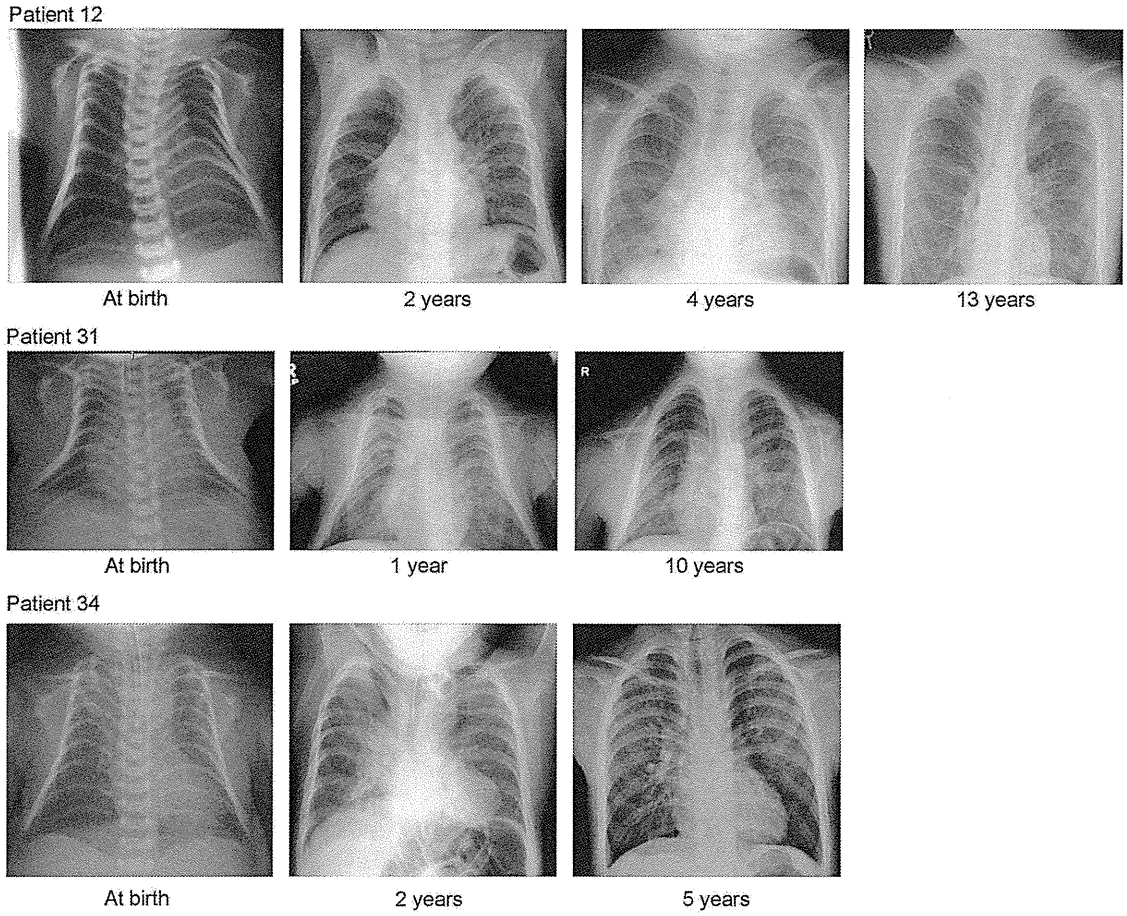

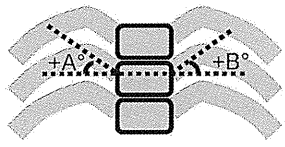

CHA = (A + B) ÷ 2
(6th posterior ribs)

M/W ratio = a / b

		CHA	M/W ratio	
Patient 12	At birth	41	70	
	2 years	39	88	
	4 years	42	94	
	13 years	39	92	
Patient 31	At birth	35	58	
	1 year	28	80	
	10 years	29	85	
Patient 34	At birth	44	70	
	2 year	48	93	
	5 years	37	96	
UPD(14)pat	At birth	+28 ~ +45	58 ~ 80	(n=8)
	~ 5 years	+25 ~ +45	>78%	(n=3)
Controls	At birth	–11 ~ +1.9	82 ~ 89	(n=10)
	~ 5 years	–21 ~ +15	83 ~ 98	(n=10)
	~ 10 years	–9.3 ~ +20	91 ~ 100	(n=10)

Figure 2 Chest roentgenograms of patient #12 of UPD-group, patient #31 of Del-S1, and patient #34 of Del-S3. *RTL1* expression level is predicted to be ~5 times higher in patients #12 and #31, and ~2.5 times higher in patient #34. The CHA to the ribs remains above the normal range throughout the study period, whereas the M/W ratio (the ratio of the mid to widest thorax diameter) normalizes with age.

of neonatal respiratory distress syndrome, and patients #8, #30 and #33 died during a respiratory infection. Of the three patients with hepatoblastoma, patient #17 died of hepatoblastoma, whereas patient #8 died during influenza infection and patient #18 died of hemophagocytic syndrome.

Comparison among/between different groups/subtypes

Clinical findings were grossly similar among/between different groups/subtypes with different expression dosages of *RTL1* and *DLK1*. However, significant differences were found for short gestational age and long duration of tube feeding in Del-group (among three groups

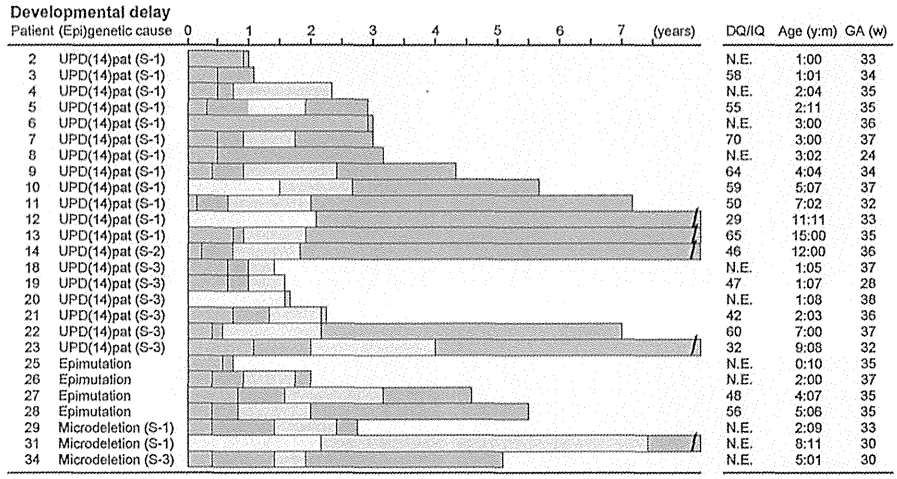

Figure 3 Developmental status. The orange, green, yellow, and blue bars represent the period before head control, the period after head control and before sitting without support, the period after sitting without support and before walking without support, and the period after walking without support, respectively. The gray bars denote the period with no information. DQ, developmental quotient; IQ, intellectual quotient; N.E., not examined; Age, age at the last examination or at death; and GA, gestational age.

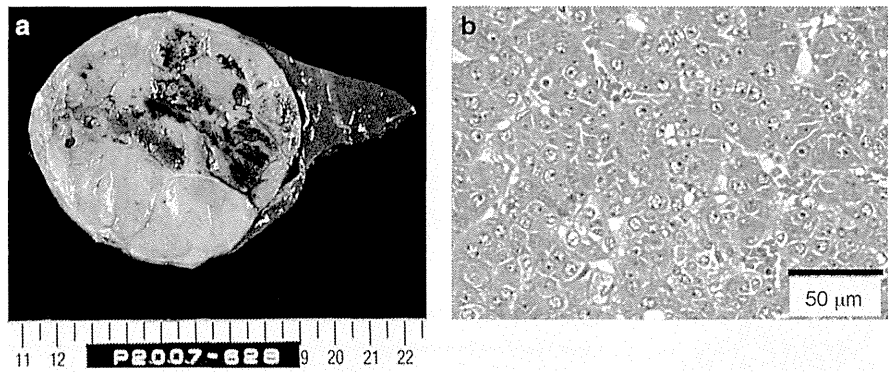

Figure 4 Hepatoblastoma in patient #8 of UPD-group. (**a**) Macroscopic appearance of the hepatoblastoma with a diameter of ~8 cm. (**b**) Microscopic appearance of the hepatoblastoma exhibiting a trabecular pattern. The hepatoblastoma cells are associated with eosinophilic cytoplasm and large nuclei, and resemble fetal hepatocytes.

and against Epi-group and UPD-group) and infrequent hairy forehead in Epi-group (among three groups and against UPD-group) (actual *P*-values are available on request).

DISCUSSION

We examined detailed clinical findings in patients with UPD(14)pat and related conditions. The results indicate that the facial features with full cheeks and protruding philtrum and the thoracic roentgenographic findings with increased CHAs to the ribs represent the pathognomonic features of UPD(14)pat and related conditions from infancy through the childhood. In addition, the decreased M/W ratios also denote the diagnostic hallmark in infancy, but not after infancy. Although other features such as polyhydramnios, placentomegaly, and abdominal wall defects are characteristic of UPD(14)pat and related conditions, they would be regarded as rather nonspecific features that are also observed in other conditions such as Beckwith–Wiedemann syndrome (BWS) (Supplementary Table S4).[12,13]

Such body and placental features were similarly exhibited by patients of each group/subtype, including those of Del-S1, Del-S2, and Del-S3 with different expression dosage of *DLK1* (1× or 2×) and *RTL1* (~2.5× or ~5×), except for patient #32 of Del-S2 who showed typical body features but apparently lacked placental features. Indeed, the difference in the *DLK1* expression dosage had no discernible clinical effects, although mouse *Dlk1* is expressed in several fetal tissues, including the ribs.[14,15] Similarly, in contrast to our previous report which suggested a possible dosage effect of *RTL1* expression level on the phenotypic severity,[2] the difference in the *RTL1* expression dosage turned out to have no recognizable clinical effects after analyzing long-term clinical courses in the affected patients. This suggests that ~2.5× *RTL1* expression is the primary factor for the phenotypic development in the body and placenta. Consistent with the critical role of excessive *RTL1* expression in the phenotypic development, mouse *Rtl1* is clearly expressed in the fetal ribs and skeletal muscles (Supplementary Figure S5) as well as in the placenta,[16,17] and human *RTL1* mRNA and RTL1 protein are strongly expressed in placentas with UPD(14)pat.[6] Thus, lack of placental abnormalities in patient #32 can be explained by assuming a positive *RTL1as* expression and resultant normal (1×) *RTL1* expression in the placenta (Supplementary Figure S1). In addition, since mouse *Gtl2* (*Meg3*) is expressed in multiple fetal tissues including the primordial cartilage,[14] this may argue for the positive role of absent *MEGs* expression in phenotypic development.